Manuscript submitted to **Biophysical** *Journal*
Article

Thermodynamics and kinetics of phase separation of protein–RNA mixtures by a minimal model

Jerelle A. Joseph[1], Jorge R. Espinosa[2], Ignacio Sanchez-Burgos[3], Adiran Garaizar[4], Daan Frenkel[5], and Rosana Collepardo-Guevara[6,*]

[1,2,3,4,6]Maxwell Centre, Cavendish Laboratory, Department of Physics, University of Cambridge, J J Thomson Avenue, Cambridge CB3 0HE
[1,2,3,4,5,6]Department of Chemistry, University of Cambridge, Lensfield Road, Cambridge, CB2 1EW
[1,2,3,4,6]Department of Genetics, University of Cambridge, Cambridge, CB2 3EH
[*]Correspondence: rc597@cam.ac.uk

ABSTRACT Intracellular liquid–liquid phase separation (LLPS) enables the formation of biomolecular condensates, such as ribonucleoprotein granules, which play a crucial role in the spatiotemporal organization of biomolecules (e.g., proteins and RNAs). Here, we introduce a patchy-particle–polymer model to investigate LLPS of protein–RNA mixtures. We demonstrate that, at low to moderate concentrations, RNA enhances the stability of RNA-binding protein (RBP) condensates because it increases the molecular connectivity of the condensed-liquid phase. Importantly, we find that RNA can also accelerate the nucleation stage of phase separation. Additionally, we asses how the capacity of RNA to increase the stability of condensates is modulated by the relative protein–protein/protein–RNA binding strengths. We find that phase separation and multiphase organization of multicomponent condensates is favored when the RNA binds with higher affinity to the lower valency proteins in the mixture, than to the cognate higher valency proteins. Collectively, our results shed light on the roles of RNA in ribonucleoprotein granule formation and the internal structuring of stress granules.

SIGNIFICANCE The interior of cells contains several membraneless compartments that are composed of proteins and RNA. These compartments are formed and sustained by LLPS. Here, we introduce a minimal coarse-grained model to study LLPS of protein–RNA mixtures. We find that RNA can increase the stability of phase-separated compartments by enhancing the molecular connectivity of proteins. Additionally, our results show that RNA actively recruits proteins—accelerating the nucleation and fusion stages of LLPS. Interestingly, we find that spatial segregation within protein–RNA compartments is controlled by fine-tuning the interaction strengths and stoichiometries of components. Our model, therefore, provides a useful tool for building a comprehensive mechanistic and thermodynamic view of protein–RNA LLPS.

1 INTRODUCTION

In recent years, it has become clear that liquid–liquid phase separation (LLPS) is responsible for the formation of membraneless organelles, including P granules and nuclear bodies (NBs) (1–4). These cellular bodies, often referred to as biomolecular condensates, display liquid-like properties, such as the ability to flow, coalesce, and drip (5–9), and are thought to self-assemble via condensation of proteins and other macromolecules in the cytoplasm and nucleoplasm. Specifically, multidomain proteins (5, 8, 10) and those comprising intrinsically disordered regions (IDRs) (11–14) have been shown to undergo LLPS, both in vitro and in cells. LLPS is mainly driven by multivalent protein–protein interactions (15, 16); for example, several phase-separating proteins possess low complexity domains (LCDs) that foster protein–protein condensation (2, 17, 18). Interactions with RNA (19–23) have been shown to strongly mediate LLPS; indeed, the vast majority of membraneless organelles [including nucleoli (19, 24, 25), stress granules (26, 27), P granules (13, 20, 28), and processing bodies (29, 30)] are ribonucleoprotein (RNP) granules (31–35), consisting of RNA and RNA-binding proteins (RBPs) (36). A central goal of the present work is to further elucidate one of the potential mechanisms by which RNA can enhance (or inhibit) LLPS and obtain predictive rules governing the composition of protein–RNA condensates.

In vitro experiments reveal that, although condensates are multicomponent systems, only a small subset of components may be required for LLPS (24, 37). For example, P granules are made up of several RNA and protein molecules; however, LAF-1 (a protein found in P granules) can self-associate into droplets that resemble P granules in vitro (13). In some cases, macromolecules that undergo LLPS may bind to and

recruit other molecules to phase-separated droplets. Landmark work by Banani and collaborators (38) showed that polySUMO and polySIM proteins assembled into droplets when mixed, and subsequently recruited fluorescently labeled SIM and SUMO monomers, respectively, to the condensates. Components, such as polySUMO and polySIM, that drive LLPS are often classified as 'scaffolds', and molecules that partition into droplets formed by scaffolds (e.g., SIM and SUMO monomers) are termed 'clients' (38). Scaffold and client stoichiometric ratios, valencies, and binding affinities have been postulated as crucial in compositional control of membraneless organelles (38).

Importantly, RNA molecules can be selectively recruited to condensates, and this recruitment is tuned by several factors including RNA length, flexibility, and shape (12, 22, 39, 40). For instance, some RNA-binding proteins contain structured RNA-binding regions—including certain RNA recognition motifs (RRMs) and zinc fingers—that bind to specific RNA sequences and drive phase separation (22, 41). In other cases, RBPs recruit RNA in a nonspecific manner (e.g., via IDRs and arginine rich regions) (20, 36, 42); thereby, partitioning RNA molecules into phase-separated droplets. Still several RBPs may contain sites for both specific and nonspecific RNA-binding (36, 41, 43, 44). Accordingly, RNA polymers tend to mimic LCDs—exhibiting multivalence character and high propensity for adopting numerous conformations that promote condensation (23). In general, RNA valence increases with length, and longer RNAs have been found to drive stress granule formation (26). Additionally, the RBP-to-RNA ratio is also very important; with the high RNA ratios suppressing LLPS and lower RNA concentrations promoting LLPS of several proteins (21, 36, 41, 43, 45). In the latter case, RNA molecules may essentially act as scaffolds for LLPS. To better understand the interplay between these and other factors, we, therefore, require biophysical models that can investigate the phase behavior of RBP–RNA mixtures.

Polymer physics provides key rules for predicting phase behavior of polymeric systems (46). For a given homopolymer–solvent mixture, the system produces two phases (i.e., a dense, polymer-rich phase and a dilute, solvent-rich phase) when the enthalpy of mixing exceeds the entropy of mixing. Flory-Huggins Theory quantifies the entropic and enthalpic terms of such systems and estimates the critical condition for phase separation (47, 48). Subsequent to these works, analytical (14, 49–56) and mean-field theoretical approaches (57–60) have been developed to study phase behavior of charged polymers and IDPs. Additionally, sequence-dependent continuum models (61–65) have been designed for probing biomolecular phase behavior. These models have proved extremely useful in identifying correlations between protein sequence and LLPS. Minimal continuum models (66–74) (including patchy-particle models) (68–73) and lattice-based approaches (16, 75–79) (notably "stickers-and-spacers" representations) (16, 75, 77) have significantly complemented and augmented these studies—revealing concentration-dependent features of multicomponent protein systems, aiding in the design of experimental studies on phase behavior, and accessing complete phase diagrams. The study of phase diagrams of biopolymer systems provides valuable insight in the various factors that influence phase separation. However, measuring complete phase diagrams is time consuming and the study of biomolecular phase behavior at atomic resolution is computationally expensive. Hence, approaches that simultaneously preserve important molecular and physicochemical details of LLPS and capture observable phase behavior in an efficient manner are appealing; since, they can be implemented at moderate computational cost.

Here we develop a simple coarse-grained approach that approximates key features of phase-separating RBPs and their RNA counterparts. The model is simple enough to permit simulation of phase transitions in mixtures containing thousands of proteins at low computational cost; it can be conveniently implemented; and it does not require extensive optimization of parameter sets. Using this minimal model, we investigate the effect of adding an RNA-like polymer to a pure RBP system. We find that the RNA polymer enhances the connectivity of RBPs and increases the critical temperature for phase separation. These results are consistent with experiments, where RNA was found to decrease the critical concentration for LLPS in RBP–RNA mixtures (21, 36, 41, 43). Additionally, we demonstrate that RNA-like polymers accelerate the nucleation stage of protein condensate formation. We then study competition and cooperative effects in multicomponent protein–RNA mixtures, and demonstrate how the droplet composition is tuned by the valencies, stoichiometries, and relative interaction strengths of the molecular components. Taken together, our work demonstrates the usefulness of minimal coarse-grained models in obtaining general rules governing RNA-driven LLPS and suggests possible molecular mechanisms involved in intracellular phase separation.

2 METHODS

Minimal coarse-grained model

We have developed a minimal coarse-grained model for RBPs that captures their multivalency (80) and RNA-binding ability—the two essential characteristics for LLPS of RBP–RNA mixtures—and can probe condensed-matter properties of biomolecular phase separation in an efficient manner. A key advantage of our approach is that all the potentials in our minimal protein model are continuous, and can be conveniently implemented in parallelised molecular dynamics (MD) software, which allows us to investigate systems of up to ten thousand proteins. Additionally, the design of the model eliminates the need for optimizing and storing extensive parameter sets, which ensures its utility and portability.

Our minimal model represents RBPs as hard spheres (of molecular diameter $\sigma = 3.405$ Å) decorated with attractive patches or "stickers" on their surface (Fig. 1A). We model

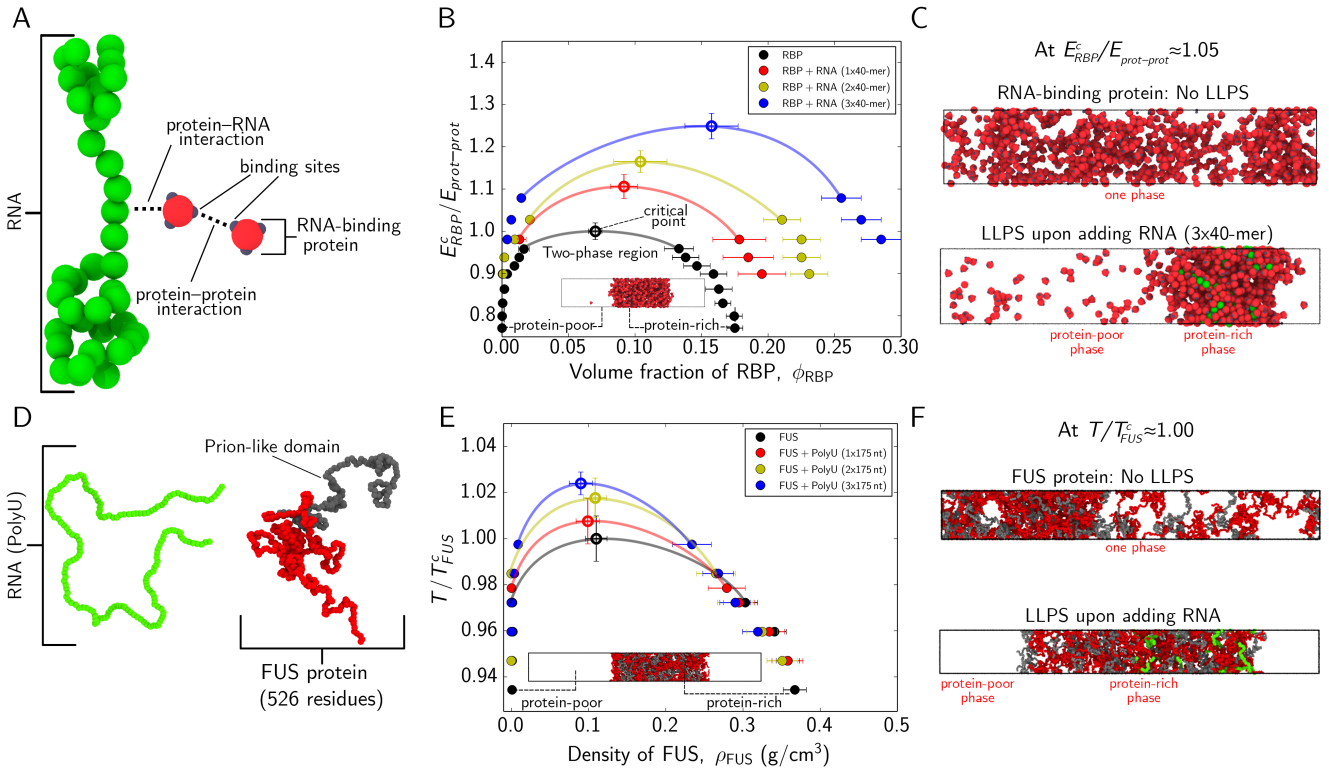

Figure 1: Obtaining phase diagrams of mixtures of RBPs and RNA. (A) Patchy-particle–polymer model for simulating interactions between proteins and RNAs. RNA is modeled as a (hard-sphere) self-avoiding polymer. RBPs are represented by hard spheres decorated with attractive patches. (B) Phase diagrams computed in terms of inverse inter-protein interaction strength ($E^c_{RBP}/E_{prot-prot}$; E^c_{RBP} is the critical inverse protein–protein interaction strength of the pure RBP) and volume fraction of the RBP (i.e., ϕ_{RBP}). In each system, 1000 RBPs were used, along with n (n = 0,1,2,3) chains of a 40-mer RNA. The densities of the dilute and condense phases are estimated from the density profiles, as described in the main text and *SI Appendix* Fig. S1. Horizontal error bars represent the standard deviations in the coexisting volume fractions. (C) Snapshots of direct coexistence simulations of RBP (top) and RBP+RNA (3x40-mer) mixture (bottom) at $E^c_{RBP}/E_{prot-prot} \approx 1.05$. (D) Residue-level coarse-grained representations of PolyU RNA and RBP FUS. In the model, each protein residue or nucleic acid is represented as a single bead (see text and *SI Appendix* for details). (E) Phase diagrams computed in terms of temperature (T/T^c_{FUS}; T^c_{FUS} is the critical temperature of pure FUS) and density of FUS (ρ_{FUS}). In each system, 24 chains of FUS were used, along with n (n = 0,1,2,3) chains of PolyU 175 nucleotides (nt) long. The densities of the dilute and condense phases are estimated from the density profiles, as described in the *SI Appendix*. Horizontal error bars represent standard deviations in the coexisting densities. (F) Snapshots of direct coexistence simulations of pure FUS (top) and FUS+PolyU (3x175 nt) mixture (bottom) at $T/T^c_{FUS} \approx 1.00$. In phase diagrams, individual critical values of the inverse $E_{prot-prot}$ (E^c) or T (T^c) are estimated by fitting the differences in ϕ_{RBP} or ρ_{FUS} (as described in ref. (80)), and corresponding critical ϕ_{RBP} or ρ_{FUS} are derived by assuming that the law of rectilinear diameters and critical exponents (81) hold in the vicinity of E^c or T^c. Uncertainties in the estimation of critical values (error bars) are obtained by performing the fitting procedure on three independent data sets.

two types of RBPs: (1) those that can drive phase separation via homotypic RBP–RBP interactions and, hence, act as scaffolds, and (2) those whose homotypic interactions are insufficient to drive phase separation and, hence, act as clients that are recruited into condensates via their interactions with the scaffolds. Based on our previous work exploring the role of valency in protein LLPS (80), we set three attractive LLPS-binding sites per scaffold RBP (3-valency RBPs), and two per client RBP (2-valency RBPs); this simple distinction allows us to capture the essential difference in the phase behavior between scaffolds and clients. Although many proteins, including RBPs, that undergo LLPS possess intrinsically disordered regions (11–14, 16, 82), our model captures the effects of protein multivalency and, therefore, approximates the way in which intrinsically disordered proteins interact with each other (72) and with RNA.

RNA molecules contain negatively charged sugar-phosphate backbones, and therefore tend to behave as self-avoiding polymers. Hence, as an extension to our previous work (80), we represent single-stranded unstructured RNAs (i.e., A- or U-rich with negligible base-pairing probability) as flexible, self-avoiding polymers (i.e., chains of hard spheres (83)) that interact with the minimal RBPs via attractive interactions (Fig. 1A). The weak attractive interactions between patchy "RBP" particles and polymers typify RBP–RNA interactions observed in biomolecular condensates (20, 21, 36, 41–43).

Direct coexistence simulations

We employ direct coexistence simulations (84–86) to compute the phase diagrams of the protein–RNA mixtures; i.e., both liquid phases are simulated via MD in the same simulation box (80). Specifically, we measure the volume fraction of the protein (Fig. 1B) in each phase as a function of the protein–protein interaction strength. The volume fraction of the RBP (ϕ_{RBP}) in a phase is defined as $\phi_{RBP} = NV_{RBP}/V \propto C_{RBP}$; where N is the total number of RBPs, V_{RBP} is the molecular volume of an RBP [i.e., 4/3 $\pi(\sigma/2)^3$], V is the total system volume, and C_{RBP} is the concentration). LLPS in cells occur over narrow temperature ranges, therefore, we assess the phase behavior of our mixtures by varying the inter-protein interaction strengths ($E_{prot-prot}$) at a fixed temperature.

At a given value of the inter-protein interaction strength, the system is simulated until the potential energy and the density profile along the box long axis have converged (*SI Appendix* Fig. S1A). LLPS is then marked by the presence of sharp interfaces (*SI Appendix* Fig. S1B). The volume fractions of the protein-rich and protein-poor phase are then computed by averaging the volume fractions (i.e., from the density profile) for the respective phases, excluding regions near the interfaces (*SI Appendix* Fig. S1B).

Hence, for a particular protein, the compositions of the coexisting protein-rich and protein-poor phases define the range of volume fractions (or concentrations) for which LLPS takes place (Fig. 1B). Having established this reference phase diagram, we then assess the effect of adding an RNA-like polymer or different proteins on the location of the phase boundaries (Fig. 1B and C). This approach allows us to obtain general rules for how proteins and RNA molecules may partition into two-liquid phases.

Further details of our patchy-particle model (80) and the simulation parameters used are found in *SI Appendix*, Sections I and II.

3 RESULTS AND DISCUSSION

Minimal model validation

Many proteins that undergo homotypic LLPS have been shown to participate in multivalent heterotypic interactions with RNA that also facilitate LLPS (36, 41, 43). For example, Molliex and coworkers (43) showed that, while RBP hnRNPA1 was able to phase-separate on its own, LLPS of hnRNPA1 was significantly enhanced in the presence of RNA. This effect was marked by a dramatic decrease in the concentration of hnRNPA1 required for phase separation (43). Similar results were also reported by Lin and colleagues (36). RNA has also been shown to drive droplet formation of RBP Whi3 (22, 41) and PGL-3 protein (20) at physiological protein concentrations.

We first employ our minimal model to probe the effects of adding RNA at low to moderate concentrations (i.e., $\phi_{RNA}/\phi_{RBP} < 15\%$) on the phase boundary of a single type of RNA binding protein (i.e., a trivalent RBP). The protein can self-associate via three binding sites on its surface and, as such, serves as a prototype for proteins that exhibit homotypically-driven LLPS. At different inter-protein interaction strengths (i.e., $11.5 \leq E_{prot-prot} \leq 14\, k_BT$), we compute the phase boundaries of the pure protein system (Fig. 1B). We then calculate the coexistence curve and the minimal interaction strength needed for phase separation (i.e., the critical point; at $E_{prot-prot} \sim 10.786\, k_BT$). Above the critical point the pure protein system forms a single well-mixed phase (Fig. 1C, top panel). At larger interaction strengths (i.e., below the critical point), the system separates into a protein-rich and protein-poor phase (Fig. 1B).

We then add a polymer that mimics an intrinsically disordered RNA chain (i.e., a self-avoiding (83) fully flexible polymer made up of 40 monomeric units; 1x40-mer) that interacts with the RBPs via moderately weak attractive interactions ($E_{prot-RNA} \sim 3\, k_BT$). We choose this polymer length, since it allows us to achieve a low RNA-to-protein concentration (i.e., ~4–12% RNA) that is consistent with experiments (20, 36, 43), while obtaining marked trends for how RNA affects protein LLPS. We then simulate the new RBP–RNA mixture above the critical point of the pure system (Fig. 1B), where the RBP can no longer sustain LLPS on its own. Note that to assess directly how effectively the RBP condenses in the presence of the RNA-like polymer, we compute our phase

diagrams in terms of the volume fraction of the RBP, as opposed to assessing the combined volume fraction of the RBP and RNA. Consistent with experimental studies of RBP–RNA mixtures (20, 22, 36, 41, 43), the RNA-like polymer promotes phase separation of the trivalent RBP; i.e., a higher critical inverse interaction strength and a broader coexistence region is obtained for the mixture versus the pure protein system (red curve in Fig. 1B).

As in the case of the Whi3–RNA mixture (22, 41), the trivalent RBPs interact with the RNA polymer via different sites than those used for protein–protein association. This suggests that the RNA polymer acts as a high-valency molecule that effectively enhances the connectivity of the protein liquid network. Indeed the average number of protein–protein bonds in the RBP condensate increases fourfold when three 40-mer RNA-like polymers are added to the RBP system at an inter–protein interaction strength of 11 k_BT (Fig. 2). Experiments and simulations have recently demonstrated that increasing the protein valency raises the critical temperature for phase separation (16, 72). These findings are consistent with earlier predictions by Bianchi et al. (87). Li et al. (5) also obtained a strong correlation between the phase boundary and the valency of interacting molecules for engineered $SH3_m$-PRM_n protein mixtures. Importantly, Rao and Parker (88) demonstrated that mRNA enhanced P-body assembly by providing multiple interaction sites for certain P-body proteins. Moreover, mutations that hindered RNA-binding suppressed P-body formation (88). Ries et al. (89) recently showed that polymethylated mRNAs can act as multivalent scaffolds for binding certain proteins and driving LLPS.

We also test whether multiple RNA-like polymers can also enhance LLPS. Thus, in addition to the original RBP—RNA mixture, we study the phase behavior for systems containing two (2x40-mer) and three (3x40-mer) RNA-like chains. Within our model, we obtain a monotonic increase in the critical point for LLPS and a widening of the coexistence region Fig. 1B. Thus, in all cases tested, the RNA-like polymer enhances LLPS of our patchy RBPs. We note that, by construction, our model is only valid at low to moderate RNA concentrations, where our approximation that RNA behaves as a self-avoiding polymer (rather than exhibiting long-range repulsion) and the assumption that RNA does not compete for RBP—RBP binding sites are reasonable. In other words, the monotonic LLPS enhancement we observe is not expected to hold at high RNA concentrations.

To verify the preceding predictions obtained via the minimal model, we investigated the effects of PolyU RNA on the phase behavior of the ALS-associated RBP fused in sarcoma (FUS). FUS is an ideal example of an RBP that can both undergo LLPS on its own via homotypic interactions (17, 90, 91) and exhibit phase separation enhancement (i.e., undergo LLPS at low protein concentrations) in the presence of a low to moderate concentrations of RNA (92–94). Using a reparameterization (65) of the residue-level coarse-grained model of Dignon et al. (61) (Fig. 1D), we compute the phase diagram of the pure FUS system (Fig. 1E), and then probe the impact of adding moderate concentrations of PolyU [modeled using the parameters proposed in ref. (95)]. For the high-resolution simulations, each residue/nucleic acid is represented by a single bead (with associated hydrophobicity, mass, and charge); therefore, we are able to delineate which protein/RNA regions drive LLPS.

Consistent with experiments (17, 90, 91), we observe that FUS phase separates due to homotypic interactions—mainly via hydrophobic PLD–PLD (PLD = prion-like domain) interactions and cation–π interactions between Tyr residues in the PLD and Arg residues in RGG (RGG = Arg-Gly-Gly rich regions) domains (see *SI Appendix* Fig. S2B). Importantly, when we add increasing amounts of PolyU, we observe that the critical temperature of the mixture also exhibits a monotonic increase, by 0.8–2.4% for 1–3 chains of 175 nt (Fig. 1E), which implies that addition of RNA permits phase separation of FUS at higher temperatures, where the phase separation of FUS alone is unfavorable. Since temperature in the coarse-grained model directly impacts the relative strength of protein–protein interactions, this result also suggests that addition of RNA would permit the formation of FUS condensates under other unfavorable LLPS conditions (e.g., salt, pH, etc). Unlike our minimal model, the residue-level coarse-grained model considers explicitly the electrostatic repulsion among RNA chains and the competition of RNA for specific scaffold–scaffold binding sites—e.g., it accounts for arginine-rich regions being utilized for FUS–FUS interactions, as well as for FUS–RNA interactions. Therefore, it can be used to investigate the role of higher concentrations of RNA in FUS condensates. These analyses reveal that higher RNA concentrations dissolves the FUS condensates (*SI Appendix* Fig. S3), as observed experimentally (21).

If we compare the phase diagrams computed with both models at low to moderate concentrations of RNA, we observe that both predict an increase in the size of the coexistence region upon insertion of RNA (Fig. 1B and E). However, the condensed-branch of the residue-level coarse-grained phase diagrams (Fig. 1E) do not exhibit the marked increase in density upon insertion of the PolyU chains predicted by our minimal model (Fig. 1B). Although both models predict an enhancement in the connectivity of FUS proteins due to addition of PolyU (see Fig. 2B), our minimal model overestimates such enhancement. We note that the residue-level model likely describes the experimental phase behavior of FUS–RNA mixtures better because it accounts more adequately for the actual size, shape, flexibility, and chemical identity of the different molecular species involved in LLPS.

However, while our minimal model was designed to study general features of RBPs–RNA LLPS, it can be conveniently parameterized to study specific protein–RNA systems (such as FUS–RNA mixtures) more intimately. For example, whereas in the current study the RNA-like polymer interacts with RBPs in a nonspecific manner, selective binding can be introduced in the model via simple pairwise definitions. Despite the

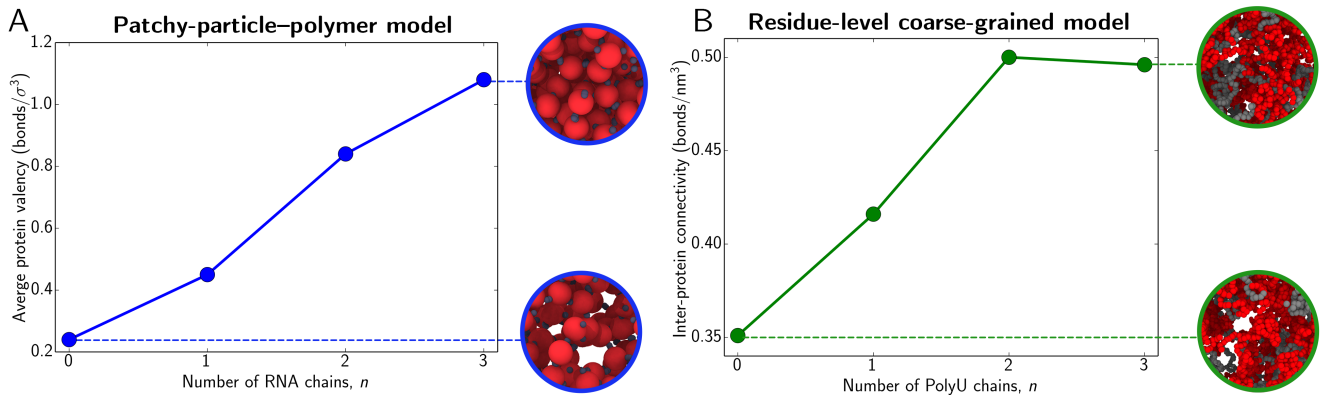

Figure 2: RNA enhances the average valency of RNA-binding proteins. Systems in (A) and (B) are identical, in terms of composition, to those in Fig. 1B and E. (A) Average protein valency (bonds/σ^3) as a function of number of RNA chains (n), computed via the patchy-particle–polymer model at an inter-protein interaction strength (i.e., $E_{prot-prot}$) of 11 k_BT. The density of each system was first equilibrated to the coexisting density of the condensed-liquid branch of their respective phase diagram (i.e., without interfaces). The systems were then simulated in the NVT ensemble to determine the average protein valency in the droplet. (Right panel) Zoomed-in snapshots of some RBPs within the simulation box showing differences in inter-protein connectivity. For clarity, the RNA-like polymers not depicted in the uppermost snapshot. (B) Inter-protein connectivity (bonds/nm^3); bonds correspond to inter-protein or protein–RNA contacts, as described in the *SI Appendix*) versus number of PolyU chains (n), computed via the reparameterized residue-level coarse-grained model (61, 65, 95) at 393 K. The systems were prepared as in (A); i.e., isotropic NpT simulations, followed by NVT ensemble computations to measure the droplet inter-protein connectivity. (Right panel) Zoomed-in snapshots of some FUS proteins within the simulation box showing differences in inter-protein connectivity. For clarity, the PolyU chains are not depicted in the uppermost snapshot. In (A) and (B) error bars (i.e., standard error) are of the same size or smaller than the symbols.

limitations of a minimal approximation, the preceding residue-level study demonstrates the usefulness of a minimal model in capturing qualitative trends of RNA-driven LLPS at low to moderate RNA concentrations. Therefore, in what follows, we exploit the advantage of the minimal model to access the sufficiently large system sizes and long timescales needed to elucidate the thermodynamic and kinetic mechanism of RNA-driven RBP LLPS. We then present a comprehensive look at the regulation of condensate stability by RNA, and how this is modulated by the addition of different types of proteins to the RBP–RNA condensates.

Moderate RNA concentrations accelerate the nucleation and growth of RBPs condensates

Beyond increasing the size of the coexistence region by connectivity-enhancement, the question is: how is the thermodynamic and kinetic mechanism of RBP LLPS impacted by RNA? To investigate this, we define a "protein cluster size" order parameter Q, that measures the average number of proteins in a given protein cluster (i.e., Q loosely describes the size of the emerging protein condensates) throughout our simulations. We first determine whether a protein is in a diluted or condensed region by employing a nearest neighbor criterion (96); wherein, proteins are assigned to condensed regions if, within a cutoff distance of 1.26 σ, they have at least three neighbors. Once all proteins are assigned, two proteins are considered to be part of the same condensed region (i.e, protein cluster) if they are separated by less than 1.26 σ from each other. The size of the largest protein cluster (Q_1), therefore, probes the nucleation potential of the system. We first computed Q_1 at different inter-protein interaction strengths for the pure protein system and in the presence of one–three 40-mer RNA-like polymers (Fig. 3A). The critical protein–protein interaction strength (10.786 k_BT) for the pure protein system is indicated on the figure (i.e., vertical dashed line). Below this threshold (i.e., left of the vertical line), the largest cluster in the pure RBP system contains about 50 proteins. At a given inter-protein interaction strength, the size of the largest protein cluster increases monotonically as more RNA-like polymers are added. Strikingly, there is a 10-fold increase in the size of the largest protein cluster (ca. 600 proteins) upon adding three 40-mer RNA-like polymers at inter-protein interaction strengths where the pure RBP does not phase separate (i.e., below 10.786 k_BT). Additionally, when RNA is added, we obtain a gain (of approximately 1 k_BT) in the stability of protein clusters. It follows that RNA effectively recruits numerous protein molecules and increases the thermodynamic stability of protein clusters.

We then probe the evolution of the two largest protein clusters (denoted Q_1+Q_2) as a function of time (Fig. 3B). In the early stages of condensation, protein clusters have a tendency to fuse and segregate often, and so the number of proteins in the two largest clusters is a more robust condensation

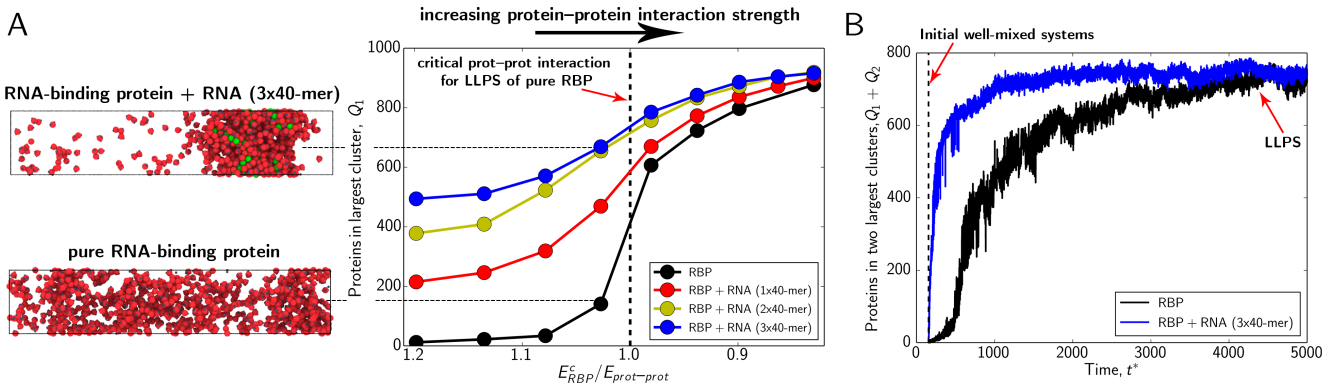

Figure 3: Thermodynamics and kinetics of protein cluster formation. (A) For a system containing 1000 RBPs, we measure the number of RBPs in the largest equilibrium cluster (Q_1) versus the protein–protein interaction strength ($E_{prot-prot}$). We then add n (n = 1,2,3) chains of a 40-mer RNA-like polymer and again measure the size of the largest protein cluster. The horizontal axis is scaled based on the critical inverse protein–protein interaction strength for LLPS of the pure RBP ($1/E^c_{RBP}$; vertical dashed line). At a protein–protein interaction strength of 10.5 k_BT (or $E^c_{RBP}/E_{prot-prot} \approx 1.05$), snapshots of the RBP+RNA (3x40-mer) mixture (top) and the pure RBP (bottom) are shown in the leftmost panel. A large distinct protein cluster forms in the RBP–RNA mixture versus smaller dispersed clusters in pure protein system. (B) For the pure RBP (black curve) and the RBP+RNA (3x40-mer) mixture (blue curve), we evaluate the number of RBPs in the two largest clusters ($Q_1 + Q_2$) as a function of time (t^*; as defined in the *SI Appendix*) at an inter-protein bond strength of 12 k_BT (or $E^c_{RBP}/E_{prot-prot} \approx 0.90$). Left of the vertical dashed line both systems exist as well-mixed fluids. Both systems equilibrate to form phase-separated condensates (i.e., LLPS).

parameter than just Q_1. To obtain a homogeneous distribution of proteins in the simulation box, we initially zeroed all attractive interactions in each system. We then activate all attractive interactions; setting the protein–protein interaction strength to a value where both systems undergo LLPS (i.e., 12 k_BT). Therefore, $Q_1 + Q_2$ versus time directly measures the speed of condensate formation. We find that the two largest condensates form approximately four times faster in the presence of the polymer (i.e., 3x40-mer RNAs) than in the pure system. Furthermore, whereas the condensate grows in a roughly monotonic fashion in the RBP–RNA mixture (blue curve in Fig. 3B), condensate sizes fluctuate to a greater extent (black curve in Fig. 3B) in the absence of the RNA.

Our simulations explain the origin of these important differences in the kinetic mechanism of condensate formation in the absence and presence of RNA. In the absence of RNA, RBPs initially form many small protein-rich nuclei. Growth of these small nuclei is dependent on their capacity to outcompete one another for binding to the free RBPs that remain in the diluted phase, and/or are undergoing fusion among themselves. This competition, along with time needed for fusion of many clusters, effectively slows down the condensation process, and results in the initial lag-time we observe, before the exponential growth rate begins (black curve in Fig. 3B). In contrast, when RNA is present, we observe formation of only a few dominant nuclei (i.e., as many clusters as there are RNA strands), which reduces competition and facilities their growth and dominance. This results in RNA considerably accelerating the formation rate of the equilibrium condensate, and a negligible lag time (blue curve in Fig. 3B).

Therefore, in addition to increasing the stability of condensates, RNA promotes LLPS by accelerating the nucleation and growth of condensates. In the literature, Falahati et al. (25) proposed a seeding mechanism for the formation of the nucleolus. Specifically, they reported that rRNA transcription precedes nucleolus assembly (25), which subsequently recruits and localizes nucleolar proteins–fostering protein cross-linking and eventual condensation. Our results are consistent with these findings; demonstrating that RNA may drive RBP condensation by facilitating the formation of the first condensate nuclei (even in conditions where RBPs alone cannot nucleate), and also by accelerating the growth of such nuclei once formed (with respect to the rate of growth of RBPs alone).

Ability of RNA to increase condensate stability depends on the composition of the system

Banani and coworkers (38) provided an initial framework to explain compositional control of membraneless organelles. Specifically, they demonstrated how low valency molecules (termed clients) can be recruited to condensates by binding to scaffolds (molecules that can phase separate on their own). They also highlighted that the valencies and relative concentrations of scaffolds and clients played significant roles in dictating the final droplet composition. In another study, Saha et al. (20) found that competition among certain proteins for RNA-binding sites altered P granule-like droplet composition.

Here, we investigate how RNA may affect condensate

stability in systems containing different types of proteins. In particular, we examine cooperation and competition effects in multicomponent mixtures comprising scaffolds, clients, and low concentrations of RNA. First, we consider the case of an intracellular mixture containing scaffolds and clients. Clients are defined as low valency proteins that cannot phase separate on their own (i.e., via homotypic client–client interactions); importantly, clients can be trafficked into the condensates by binding with high-affinity at the same sites used for homotypic scaffold–scaffold interactions. The protein composition of this mixture is 64% scaffolds (trivalent proteins; Fig. 4A) and 36% clients (divalent proteins; Fig. 4A)—i.e., the mixture contains a scaffold-to-client ratio of 1.78—and all inter-protein interaction strengths are equivalent. Notably, in comparison to the pure RBP (in Fig. 1B), this mixture shows reduced propensity to phase separate (i.e., a drop in the critical inverse protein–protein interaction strength by ∼7%; see *SI Appendix* Fig. S3). This result agrees well with the original scaffold–client model (38) predictions, and is further supported by previous computational (68) and experimental work (69). For example, Nguemaha and Zhou (68) demonstrated that regulators of LLPS (analogous to clients in this case) may lead to suppression of driver (i.e., scaffolds) phase separation if regulator–driver binding affinities are comparable to driver–driver ones. In this scenario, regulators/clients displace drivers/scaffolds from the condensate at the expense of weakening the strength and connectivity of the percolated network (68, 72).

We then add RNA to the reference scaffold–client mixture, and investigate whether RNA enhances LLPS of this system. In particular, we consider the case where, in addition to scaffolds, clients bind to RNA with high affinity. To probe the effects of RNA, we simulate the mixture very close to the critical protein–protein interaction strength of the reference client-scaffold mixture (i.e., 11.75 k_BT; see *SI Appendix* Fig. S4 and Fig. 4B). Upon equilibration, no LLPS is observed (Mixture I in Table 1; Fig. 4C); i.e., absence of sharp and well-defined interfaces. Interestingly, the RNA-like polymer is almost entirely coated by scaffolds (∼84%), despite the binding strength of both client and scaffold proteins with the RNA being equal (Table 1). This disparity in the type of proteins coating the polymer strongly suggests that the dissociation constants for the higher valency scaffolds (that can form more bonds with surrounding molecules) are smaller. Thus, higher valency RBPs have a greater probability of remaining bound to RNA (and bound in the percolating network).

Consequently, in a mixture containing both RNA-binding scaffolds and RNA-binding clients, RNA shows a preference for interacting with the scaffolds (even though in our model both scaffold–RNA and client–RNA bonds have the same interaction strength by construction). On similar grounds, scaffolds preferentially associate with adjacent scaffolds, creating a higher concentration of clients in the remaining mixture. We quantify the scaffold-to-client ratio in the remaining mixture (i.e., the effective ratio) by considering all proteins in the system, except those that are directly coating the RNA polymer. This quantity allows us to estimate the amount of scaffolds that are available for binding to (and recruiting) clients. In Mixture I, we find that the effective scaffold-to-client ratio decreases by ∼7% with respect to the reference mixture. Our recent work (72) demonstrates that the addition of low-valency clients that are strong competitors for scaffold–scaffold interactions (like the ones in Mixture I) decreases the stability of condensates by diminishing the connectivity of the liquid network, and that this effect is amplified as the scaffold-to-client ratio decreases. Therefore, in the presence of strong-competing clients and with a limited amount of scaffolds, RNA indirectly decreases the connectivity of the condensed liquid by essentially reducing the effective scaffold-to-client ratio. Hence, the net effect is that droplet formation is not enhanced in the presence of RNA; indeed, the size of the largest protein cluster (Q_1) decreases by ∼3% when the RNA-like polymer is added to the mixture. Conversely, we find that when clients do not compete for scaffold binding sites a reduction in the effective scaffold-to-client ratio does not inhibit LLPS (*SI Appendix* Fig. S5); since clients cannot replace LLPS-stabilizing scaffold–scaffold connections with LLPS-inhibiting scaffold–client ones.

Next, we test the effect of the RNA-like polymer on the phase behavior of a mixture of RNA-binding scaffolds and non-RNA-binding clients (i.e., the interaction strength between the client proteins and the RNA is set to zero; Mixture II in Table 1 and Fig. 4D). Clients compete with the RNA polymer (and with the scaffolds themselves) for binding to the scaffold proteins. However, clients are now unable to bind directly to the RNA polymer; hence, upon equilibration, ∼99% of the molecules coating the RNA polymer are scaffolds. The interaction of scaffolds with RNA and adjacent scaffolds effectively decreases the ratio of available scaffolds to clients by ∼13% with respect to the reference mixing ratio. There are effectively more clients in the remaining mixture that compete strongly with scaffolds for scaffold–scaffold binding sites; hence, the more LLPS-stabilizing scaffold–scaffold connections are replaced by connectivity-diminishing scaffold–client ones. Thus, the size of the largest protein cluster diminishes (i.e., $\Delta Q_1 \approx -7\%$) and droplet formation is not enhanced (Mixture II in Table 1). In fact, the reduction in the size of the largest protein clusters (i.e., nucleation is suppressed) in Mixtures I and II suggests that the RNA inhibits phase separation in these systems.

Finally, we assess the effects of RNA on the phase boundaries of a mixture of non-RNA-binding scaffolds and RNA-binding clients (i.e., we switch off the attractive interaction between the scaffolds and the RNA; Mixture III in Table 1). Addition of the RNA-like polymer increases the size of the largest protein cluster by ∼7%. RNA enhances LLPS of this system (Fig. 4E) because it exclusively recruits clients and effectively sequestrates them away from scaffolds. Accordingly, RNA decreases the availability of clients that would otherwise compete with scaffold self assembly. Hence, droplet formation

Table 1: We start with a reference mixture containing 64% (768 trivalent proteins) scaffolds and 36% (432 divalent proteins) clients (i.e., a ref. scaffold-to-client ratio of 1.78) that can undergo LLPS. We then add a 40-mer RNA at an inter-protein interaction strength of 11.75 k_BT (i.e., close to the critical protein–protein interaction strength of the original scaffold–client mixture), modulate the cross interactions between the mixture components, and analyze whether the RNA polymer enhances LLPS reference of the mixture. To assess the ratio of scaffolds to clients remaining after coating the RNA, we consider all scaffolds and clients that are not directly bound to the RNA polymer. The change in this ratio is computed with respect to the 1.78 reference value. We also assess the change in Q_1 (number of scaffolds and clients in the largest cluster) to quantify the enhancement or inhibition of LLPS of the mixture upon adding RNA. Snapshots of observed phase behaviors are given in Fig 4.

Mixture	**I**	**II**	**III**
client–scaffold interaction?	yes	yes	yes
client–RNA interaction?	yes	no	yes
scaffold–RNA interaction?	yes	yes	no
proteins coating RNA	84±0.5% scaffolds	99±0.5% scaffolds	1±0.5% scaffolds
scaffold-to-client ratio after RNA coating	1.65±0.01	1.55±0.01	2.27±0.01
change in scaffold-to-client ratio	-7±0.5%	-13±0.5%	+28±0.5%
variation in size of largest protein cluster (ΔQ_1)	-3±1%	-7±1%	+7±1%
RNA enhances LLPS?	no	no	yes

is promoted when RNA shows a preference for clients; in this final mixture, clients constitute ~99% of the molecules coating the RNA polymer. Ergo, the effective ratio of scaffolds-to-clients increases; ensuring that there are sufficient free-binding sites on the scaffolds to foster scaffold–scaffold interactions and phase separation.

Mixing non-RNA-binding scaffolds and RNA-binding clients with RNA yields multiphase condensates with a marked spatial segregation of the RNA and associated clients in the condensate (Fig. 4E); in contrast to the binary RNA-binding scaffold–RNA mixture (i.e., without clients), where the RNA is embedded within the liquid drop (bottom panel in Fig. 1C), the client-coated RNA is now located near the droplet interface. Even in the other mixtures (Fig. 4C and 4D), where no marked protein phase separation is observed, the RNA is, in general, uniformly coated by the surrounding proteins. This spatial segregation can be rationalized from the smaller contribution that low valency proteins are expected to have to the interfacial free energy and the melting enthalpy of condensates (37, 97, 98). Consequently, the client-coated RNA migrates to the edge of the condensate to minimize both the interfacial free energy of the system and the chemical potential of the droplet.

Overall, we find that spatial segregation of species within condensates leading to multiphase condensates can be achieved in multicomponent mixtures, and is controlled by fine-tuning the effective scaffold-to-client ratio and interaction strengths among species. Our results agree well with recent experiments where it is reported that different polymers partition into multiphase droplets depending on the relative interactions between mixture components (99, 100). Such multiphase segregation within condensates has also been reported for mixtures of model IDPs and RNA (97), as well as the nucleolus (37) and stress granules (101), where internal structuring into various sub-compartments (e.g., a core-shell) may arise. Hence, the present model may prove useful in advancing our understanding of LLPS into multiphase biomolecular condensates.

CONCLUSIONS

In this work, we have introduced a patchy-particle–polymer model capable of probing LLPS in protein–RNA mixtures from a mechanistic and thermodynamic point of view. Specifically, we have studied the effects of RNA: (*i*) on phase separation of model RBPs, (*ii*) on the thermodynamics and kinetics of condensate formation, and (*iii*) in the stability of multicomponent phase-separated protein–RNA mixtures. From our simulations, fundamental rules/features relating to LLPS in these systems emerge, at low to moderate RNA concentrations: (1) RNAs can act as high-valency molecules that promote phase separation by increasing the effective valency (i.e., connectivity) of RBPs (scaffolds); (2) RNA molecules increase the stability of condensates and accelerate the nucleation process; (3) addition of RNA to phase-separated scaffold–client (low-valency proteins) mixtures can lead to suppression of LLPS due to competition between RNA and clients for scaffold binding sites; (4) spatial segregation of components within phase-separated protein–RNA droplets is controlled by fine-tuning the effective ratio of scaffold to client proteins and interaction strengths of components. In particular, our work suggests that inhomogeneous cellular bodies may form at low RNA concentrations, when the RNA polymer exhibits a higher affinity for client proteins than for scaffolds.

Our findings provide an account of how low to moderate concentrations of RNA can significantly enhance phase separation of RNA binding proteins—enabling LLPS even under unfavorable conditions (e.g., super critical temperatures,

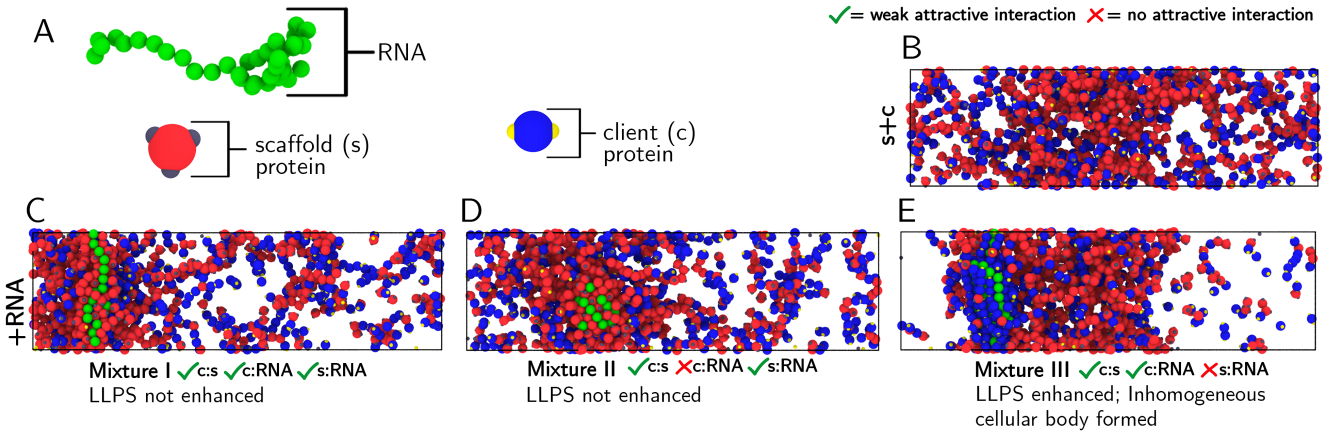

Figure 4: Composition of biomolecular condensates is regulated by the relative interaction strengths of molecular components. (A) Depiction of clients (divalent proteins), scaffolds (trivalent proteins) and a 40-mer RNA. (B) Reference client–scaffold mixture composed of 36% divalent proteins (clients) and 64% trivalent proteins (scaffolds) at an inter-protein interaction strength of 11.75 k_BT. (C)–(E) Phase behavior of client–scaffold–RNA mixtures (i.e., Mixtures I–III) described in Table 1.

extreme pHs, subsaturation protein concentrations)—and postulates the high-valency of RNAs as the molecular origin of such enhancement. The high-valency of RNA is a critical modulator of RBP LLPS because it augments the molecular connectivity of condensates (thereby increasing their stability), and increases the enthalpic gain of bringing many RBPs in close contact to form the first nuclei. The mechanisms proposed here to explain how the influence of RNA on the phase behavior of RNA-binding proteins can be used to guide the design of in vitro experiments. Together, our work provides a useful tool for interrogating protein–RNA systems, and for elucidating mechanisms of intracellular liquid–liquid phase separation.

AUTHOR CONTRIBUTIONS

J.A.J., J.R.E., D.F., and R.C.-G. designed the research; J.A.J., J.R.E., I.S.-B., and A.G. performed the simulations; J.A.J., J.R.E., I.S.-B., and A.G. analyzed the data; J.A.J., J.R.E., D.F., and R.C.-G. wrote the manuscript; and R.C.-G. supervised the research.

ACKNOWLEDGMENTS

We thank Jeetain Mittal and Gregory L. Dignon for invaluable help with the implementation of their sequence-dependent protein coarse-grained model. This project was funded by the European Research Council (ERC) under the European Union Horizon 2020 research and innovation programme (grant agreement No 803326). J.A.J. is a King's College Research Fellow. J.R.E. is an Oppenheimer Research Fellow and an Emmanuel College Research Fellow. I.S.-B. acknowledges Oppenheimer funding, an Engineering and Physical Sciences Research Council (EPSRC) scholarship, and an Emmanuel College Derek Brewer scholarship. A.G. is funded by an EPSRC studentship (EP/N509620/1). R.C.-G. is an Advanced Research Fellow from the Winton Programme for the Physics of Sustainability. This work was performed using resources provided by the Cambridge Tier-2 system operated by the University of Cambridge Research Computing Service (http://www.hpc.cam.ac.uk) funded by EPSRC Tier-2 capital grant EP/P020259/1.

REFERENCES

1. Anthony A Hyman, Christoph A Weber, and Frank Jülicher. "Liquid-liquid phase separation in biology". *Annual Review of Cell and Developmental Biology* 30 (2014), pp. 39–58.

2. Yongdae Shin and Clifford P Brangwynne. "Liquid phase condensation in cell physiology and disease". *Science* 357.6357 (2017), eaaf4382.

3. Jonathon A. Ditlev, Lindsay B. Case, and Michael K. Rosen. "Who's in and who's out—compositional control of biomolecular condensates". *Journal of Molecular Biology* 430.23 (2018), pp. 4666–4684.

4. Simon Alberti, Amy Gladfelter, and Tanja Mittag. "Considerations and Challenges in Studying Liquid-Liquid Phase Separation and Biomolecular Condensates". *Cell* 176.3 (2019), pp. 419–434.

5. Pilong Li et al. "Phase transitions in the assembly of multivalent signalling proteins". *Nature* 483 (2012), pp. 336–340.

6. Tetsuro Murakami et al. "ALS/FTD Mutation-Induced Phase Transition of FUS Liquid Droplets and Reversible Hydrogels into Irreversible Hydrogels Impairs RNP Granule Function". *Neuron* 88.4 (2015), pp. 678–690.

7. Hermann Broder Broder Schmidt and Rajat Rohatgi. “In Vivo Formation of Vacuolated Multi-phase Compartments Lacking Membranes”. *Cell Reports* 16.5 (2016), pp. 1228–1236.
8. Daxiao Sun et al. “Polyubiquitin chain-induced p62 phase separation drives autophagic cargo segregation”. *Cell Research* 28.4 (2018), pp. 405–415.
9. Miriam Linsenmeier et al. “Dynamics of synthetic membraneless organelles in microfluidic droplets”. *Angewandte Chemie International Edition* 58.41 (2019), p. 14489.
10. Sudeep Banjade and Michael K Rosen. “Phase transitions of multivalent proteins can promote clustering of membrane receptors”. *eLife* 3 (2014), e04123.
11. A Patel et al. “A Liquid-to-Solid Phase Transition of the ALS Protein FUS Accelerated by Disease Mutation”. English. *Cell* 162.5 (2015), pp. 1066–1077.
12. Timothy J. J. J Nott et al. “Phase Transition of a Disordered Nuage Protein Generates Environmentally Responsive Membraneless Organelles”. English. *Molecular Cell* 57.5 (2015), pp. 936–947.
13. Shana Elbaum-Garfinkle et al. “The disordered P granule protein LAF-1 drives phase separation into droplets with tunable viscosity and dynamics”. *Proceedings of the National Academy of Sciences* 112.23 (2015), pp. 7189–7194.
14. Yi Hsuan Lin et al. “Charge pattern matching as a ‘fuzzy’ mode of molecular recognition for the functional phase separations of intrinsically disordered proteins”. *New Journal of Physics* 19.11 (2017), p. 115003.
15. Salman F. Banani et al. “Biomolecular condensates: Organizers of cellular biochemistry”. *Nature Reviews Molecular Cell Biology* 18.5 (2017), pp. 285–298.
16. Erik W. Martin et al. “Valence and Patterning of Aromatic Residues Determine the Phase Behavior of Disordered Prion-Like Domains”. *Science* 367.6478 (2020), pp. 694–699.
17. Masato Kato et al. “Cell-free formation of RNA granules: Low complexity sequence domains form dynamic fibers within hydrogels”. *Cell* 149.4 (2012), pp. 753–767.
18. Titus M. Franzmann and Simon Alberti. “Prion-like low-complexity sequences: Key regulators of protein solubility and phase behavior”. *Journal of Biological Chemistry* 294.18 (2019), pp. 7128–7136.
19. Joel Berry et al. “RNA transcription modulates phase transition-driven nuclear body assembly”. *Proceedings of the National Academy of Sciences of the United States of America* 112.38 (2015), E5237–E5245.
20. Shambaditya Saha et al. “Polar Positioning of Phase-Separated Liquid Compartments in Cells Regulated by an mRNA Competition Mechanism”. *Cell* 166.6 (2016), pp. 1572–1584.
21. Shovamayee Maharana et al. “RNA buffers the phase separation behavior of prion-like RNA binding proteins”. *Science* 360.6391 (2018), pp. 918–921.
22. Erin M Langdon et al. “mRNA structure determines specificity of a polyQ-driven phase separation”. *Science* 360.6391 (2018), pp. 922–927.
23. Kevin Rhine, Velinda Vidaurre, and Sua Myong. “RNA Droplets”. *Annual Review of Biophysics* 49.1 (2020), pp. 247–265.
24. Diana M Mitrea et al. “Nucleophosmin integrates within the nucleolus via multi-modal interactions with proteins displaying R-rich linear motifs and rRNA”. *eLife* 5 (2016), e13571.
25. Hanieh Falahati et al. “Nucleation by rRNA Dictates the Precision of Nucleolus Assembly”. *Current Biology* 26.3 (2016), pp. 277–285.
26. Anthony Khong et al. “The Stress Granule Transcriptome Reveals Principles of mRNA Accumulation in Stress Granules”. *Molecular Cell* 68.4 (2017), pp. 808–820.
27. Briana Van Treeck and Roy Parker. “Emerging Roles for Intermolecular RNA-RNA Interactions in RNP Assemblies”. *Cell* 174.4 (2018), pp. 791–802.
28. J Smith et al. “Spatial patterning of P granules by RNA-induced phase separation of the intrinsically-disordered protein MEG-3”. *eLife* 5 (2016).
29. Ujwal Sheth and Roy Parker. “Decapping and decay of messenger RNA occur in cytoplasmic processing bodies”. *Science* 300.5620 (2003), pp. 805–808.
30. Daniela Teixeira et al. “Processing bodies require RNA for assembly and contain nontranslating mRNAs”. *RNA* 11.4 (2005), pp. 371–382.
31. Joseph G. Gall. “Cajal Bodies: The First 100 Years”. *Annual Review of Cell and Developmental Biology* 16.1 (2000), pp. 273–300.
32. Archa H. Fox et al. “Paraspeckles: A novel nuclear domain”. *Current Biology* 12.1 (2002), pp. 13–25.
33. Paul Anderson and Nancy Kedersha. “RNA granules ”. *Journal of Cell Biology* 172.6 (2006), pp. 803–808.
34. Michael A. Kiebler and Gary J. Bassell. “Neuronal RNA Granules: Movers and Makers”. *Neuron* 51.6 (2006), pp. 685–690.
35. J. Ross Buchan. “MRNP granules Assembly, function, and connections with disease”. *RNA Biology* 11.8 (2014), pp. 1019–1030.

36. Yuan Lin et al. "Formation and Maturation of Phase-Separated Liquid Droplets by RNA-Binding Proteins". *Molecular Cell* 60.2 (2015), pp. 208–219.

37. Marina Feric et al. "Coexisting Liquid Phases Underlie Nucleolar Subcompartments". *Cell* 165.7 (2016), pp. 1686–1697.

38. Salman F. Banani et al. "Compositional Control of Phase-Separated Cellular Bodies". English. *Cell* 166.3 (2016), pp. 651–663.

39. Timothy J Nott, Timothy D Craggs, and Andrew J Baldwin. "Membraneless organelles can melt nucleic acid duplexes and act as biomolecular filters". *Nature Chemistry* 8.6 (2016), pp. 569–575.

40. Stefan Schütz, Erik R Nöldeke, and Remco Sprangers. "A synergistic network of interactions promotes the formation of in vitro processing bodies and protects mRNA against decapping". *Nucleic Acids Research* 45.11 (2017), pp. 6911–6922.

41. Huaiying Y Zhang et al. "RNA Controls PolyQ Protein Phase Transitions". English. *Molecular Cell* 60.2 (2015), pp. 220–230.

42. D S W Protter et al. "Intrinsically Disordered Regions Can Contribute Promiscuous Interactions to RNP Granule Assembly". *Cell Reports* 22.6 (2018), pp. 1401–1412.

43. Amandine Molliex et al. "Phase Separation by Low Complexity Domains Promotes Stress Granule Assembly and Drives Pathological Fibrillization". *Cell* 163.1 (2015), pp. 123–133.

44. Jian Kang et al. "A unified mechanism for LLPS of ALS/FTLD-causing FUS as well as its modulation by ATP and oligonucleic acids". *PLoS Biology* 17.6 (2019), e3000327.

45. Jacob R. Mann et al. "RNA Binding Antagonizes Neurotoxic Phase Transitions of TDP-43". *Neuron* 102.2 (2019), pp. 321–338.

46. Clifford P. Brangwynne, Peter Tompa, and Rohit V. Pappu. "Polymer physics of intracellular phase transitions". *Nature Physics* 11 (2015), p. 899.

47. Paul J. Flory. "Thermodynamics of High Polymer Solutions". *Journal of Chemical Physics* 10.1 (1942), pp. 51–61.

48. Maurice L. Huggins. "Some Properties of Solutions of Long-chain Compounds." *Journal of Physical Chemistry* 46.1 (1942), pp. 151–158.

49. YH Lin et al. "Sequence-specific polyampholyte phase separation in membraneless organelles". *Physical Review Letters* 117 (2016), p. 178101.

50. Yi-Hsuan Lin et al. "Random-phase-approximation theory for sequence-dependent, biologically functional liquid-liquid phase separation of intrinsically disordered proteins". *Journal of Molecular Liquids* 228 (2017), pp. 176–193.

51. Li-Wei Chang et al. "Sequence and entropy-based control of complex coacervates". *Nature Communications* 8.1 (2017), p. 1273.

52. Yi-Hsuan Lin and Hue Sun Chan. "Phase Separation and Single-Chain Compactness of Charged Disordered Proteins Are Strongly Correlated". *Biophysical Journal* 112.10 (2017), pp. 2043–2046.

53. Jie Wang et al. "A Molecular Grammar Governing the Driving Forces for Phase Separation of Prion-like RNA Binding Proteins". *Cell* 174.3 (2018), pp. 688–699.

54. Yi Hsuan Lin, Julie D. Forman-Kay, and Hue Sun Chan. "Theories for Sequence-Dependent Phase Behaviors of Biomolecular Condensates". *Biochemistry* 57.17 (2018), pp. 2499–2508.

55. Yi Hsuan Lin et al. "A unified analytical theory of heteropolymers for sequence-specific phase behaviors of polyelectrolytes and polyampholytes". *Journal of Chemical Physics* 152.4 (2020), p. 045102.

56. Jeremy D Schmit et al. "Protein Network Structure Enables Switching between Liquid and Gel States". *Journal of the American Chemical Society* 142.2 (2020), pp. 874–883.

57. James McCarty et al. "Complete Phase Diagram for Liquid-Liquid Phase Separation of Intrinsically Disordered Proteins". *Journal of Physical Chemistry Letters* 10.8 (2019), pp. 1644–1652.

58. Scott P O Danielsen et al. "Small ion effects on self-coacervation phenomena in block polyampholytes". *Journal of Chemical Physics* 151.3 (2019), p. 34904.

59. Scott P O Danielsen et al. "Molecular design of self-coacervation phenomena in block polyampholytes". *Proceedings of the National Academy of Sciences* 116.17 (2019), 8224 LP –8232.

60. Yanxian Lin et al. "Narrow equilibrium window for complex coacervation of tau and RNA under cellular conditions". *eLife* 8 (2019), e42571.

61. Gregory L. Dignon et al. "Sequence determinants of protein phase behavior from a coarse-grained model". English. *Plos Computational Biology* 14.1 (2018). Ed. by Yanay Ofran, e1005941.

62. Gregory L Dignon et al. "Temperature-Controlled Liquid–Liquid Phase Separation of Disordered Proteins". *ACS Central Science* 5.5 (2019), pp. 821–830.

63. Suman Das et al. "Coarse-grained residue-based models of disordered protein condensates: Utility and limitations of simple charge pattern parameters". *Physical Chemistry Chemical Physics* 20.45 (2018), pp. 28558–28574.
64. Antonia Statt et al. "Model for disordered proteins with strongly sequence-dependent liquid phase behavior". *Journal of Chemical Physics* 152.7 (2020), p. 75101.
65. Suman Das et al. "Comparative Roles of Charge, π, and Hydrophobic Interactions in Sequence-Dependent Phase Separation of Intrinsically Disordered Proteins". *Proceedings of the National Academy of Sciences* (2020).
66. Kiersten M. Ruff, Tyler S. Harmon, and Rohit V. Pappu. "CAMELOT: A machine learning approach for coarse-grained simulations of aggregation of block-copolymeric protein sequences". *Journal of Chemical Physics* 143.24 (2015), p. 243123.
67. Tyler S. Harmon, Alex S. Holehouse, and Rohit V. Pappu. "Differential solvation of intrinsically disordered linkers drives the formation of spatially organized droplets in ternary systems of linear multivalent proteins". *New Journal of Physics* 20.4 (2018), p. 45002.
68. Valery Nguemaha and Huan Xiang Zhou. "Liquid-Liquid Phase Separation of Patchy Particles Illuminates Diverse Effects of Regulatory Components on Protein Droplet Formation". *Scientific Reports* 8.1 (2018), p. 6728.
69. Archishman Ghosh, Konstantinos Mazarakos, and Huan-Xiang Zhou. "Three archetypical classes of macromolecular regulators of protein liquid–liquid phase separation". *Proceedings of the National Academy of Sciences* 116.39 (2019), 19474 LP –19483.
70. Anne E Hafner, Johannes Krausser, and Anđela Šarić. "Minimal coarse-grained models for molecular self-organisation in biology". *Current Opinion in Structural Biology* 58 (2019), pp. 43–52.
71. David W. Sanders et al. "Competing Protein-RNA Interaction Networks Control Multiphase Intracellular Organization". *Cell* 181.2 (2020), pp. 306–324.
72. Jorge R. Espinosa et al. "Liquid network connectivity regulates the stability and composition of biomolecular condensates with many components". *Proceedings of the National Academy of Sciences of the United States of America* 117.24 (2020), pp. 13238–13247.
73. Meta Heidenreich et al. "Designer protein assemblies with tunable phase diagrams in living cells". *Nature Chemical Biology* 16.9 (2020), pp. 939–945.
74. Adiran Garaizar et al. "Expansion of Intrinsically Disordered Proteins Increases the Range of Stability of Liquid–Liquid Phase Separation". *Molecules* 25.20 (2020), p. 4705.
75. Tyler S. Harmon et al. "Intrinsically disordered linkers determine the interplay between phase separation and gelation in multivalent proteins". *eLife* 6 (2017), e30294.
76. Suman Das et al. "A Lattice Model of Charge-Pattern-Dependent Polyampholyte Phase Separation". *The Journal of Physical Chemistry B* 122.21 (2018), pp. 5418–5431.
77. Jeong Mo Choi, Furqan Dar, and Rohit V. Pappu. "LASSI: A lattice model for simulating phase transitions of multivalent proteins". *PLoS Computational Biology* 15.10 (2019), e1007028.
78. Nicholas A S Robichaud, Ivan Saika-Voivod, and Stefan Wallin. "Phase behavior of blocky charge lattice polymers: Crystals, liquids, sheets, filaments, and clusters". *Physical Review E* 100.5 (2019), p. 52404.
79. Daniel Nilsson and Anders Irbäck. "Finite-size scaling analysis of protein droplet formation". *Physical Review E* 101.2 (2020), p. 22413.
80. Jorge R. Espinosa et al. "Breakdown of the law of rectilinear diameter and related surprises in the liquid-vapor coexistence in systems of patchy particles". *Journal of Chemical Physics* 150.22 (2019), p. 224510.
81. John Shipley Rowlinson and Benjamin Widom. *Molecular theory of capillarity*. Courier Corporation, 2013.
82. Kiersten M Ruff, Rohit V Pappu, and Alex S Holehouse. "Conformational preferences and phase behavior of intrinsically disordered low complexity sequences: insights from multiscale simulations". *Current Opinion in Structural Biology* 56 (2019), pp. 1–10.
83. J Jover et al. "Pseudo hard-sphere potential for use in continuous molecular-dynamics simulation of spherical and chain molecules". *Journal of Chemical Physics* 137.14 (2012), p. 144505.
84. J R Espinosa et al. "On fluid-solid direct coexistence simulations: The pseudo-hard sphere model". English. *Journal of Chemical Physics* 139.14 (2013), p. 144502.
85. Ramón García Fernández, Josá L.F. F Abascal, and Carlos Vega. "The melting point of ice Ih for common water models calculated from direct coexistence of the solid-liquid interface". *Journal of Chemical Physics* 124.14 (2006), p. 144506.
86. A.J.C. Ladd and L.V. Woodcock. "Triple-point coexistence properties of the lennard-jones system". *Chemical Physics Letters* 51.1 (1977), pp. 155–159.
87. E Bianchi et al. "Phase diagram of patchy colloids: Towards empty liquids". English. *Physical Review Letters* 97.16 (2006).

88. Bhalchandra S. Rao and Roy Parker. "Numerous interactions act redundantly to assemble a tunable size of P bodies in Saccharomyces cerevisiae". *Proceedings of the National Academy of Sciences of the United States of America* 114.45 (2017), E9569–E9578.

89. Ryan J. Ries et al. "m6A enhances the phase separation potential of mRNA". *Nature* 571.7765 (2019), pp. 424–428.

90. Zhihui Sun et al. "Molecular determinants and genetic modifiers of aggregation and toxicity for the als disease protein fus/tls". *PLoS Biology* 9.4 (2011), e1000614.

91. Tina W. Han et al. "Cell-free formation of RNA granules: Bound RNAs identify features and components of cellular assemblies". *Cell* 149.4 (2012), pp. 768–779.

92. Jacob C. Schwartz et al. "RNA Seeds Higher-Order Assembly of FUS Protein". *Cell Reports* 5.4 (2013), pp. 918–925.

93. Xueyin Wang, Jacob C Schwartz, and Thomas R Cech. "Nucleic acid-binding specificity of human FUS protein." *Nucleic acids research* 43.15 (2015), pp. 7535–43.

94. Kathleen A. Burke et al. "Residue-by-Residue View of In Vitro FUS Granules that Bind the C-Terminal Domain of RNA Polymerase II". *Molecular Cell* 60.2 (2015), pp. 231–241.

95. Roshan Mammen Regy et al. "Sequence dependent phase separation of protein-polynucleotide mixtures elucidated using molecular simulations". *Nucleic Acids Research* 48.22 (2020), pp. 12593–12603.

96. Pieter Rein ten Wolde and Daan Frenkel. "Computer simulation study of gas–liquid nucleation in a Lennard-Jones system". *Journal of Chemical Physics* 109.22 (1998), pp. 9901–9918.

97. Steven Boeynaems et al. "Spontaneous driving forces give rise to protein-RNA condensates with coexisting phases and complex material properties". *Proceedings of the National Academy of Sciences* 116.16 (2019), pp. 7889–7898.

98. Tiemei Lu and Evan Spruijt. "Multiphase Complex Coacervate Droplets". *Journal of the American Chemical Society* 142.6 (2020), pp. 2905–2914.

99. Gregory A. Mountain and Christine D. Keating. "Formation of Multiphase Complex Coacervates and Partitioning of Biomolecules within them". *Biomacromolecules* 21.2 (2020), pp. 630–640.

100. Taranpreet Kaur et al. "Sequence-encoded and Composition-dependent Protein-RNA Interactions Control Multiphasic Condensate Morphologies". *bioRxiv* (2020), p. 2020.08.30.273748.

101. Saumya Jain et al. "ATPase-Modulated Stress Granules Contain a Diverse Proteome and Substructure". English. *Cell* 164.3 (2016), pp. 487–498.

SUPPLEMENTARY MATERIAL

An online supplement to this article can be found by visiting BJ Online at http://www.biophysj.org